Biosensors and Bioelectronics 224 (2023) 115052

Contents lists available at ScienceDirect

Biosensors and Bioelectronics

journal homepage: www.elsevier.com/locate/bios

A cathodic photoelectrochemical immunoassay with dual signal amplification for the ultrasensitive detection of DNA damage biomarkers

Bihong Zhang [a,b], Fangfang Li [a,b], Linyu Shen [a,b], Lu Chen [b,c], Zhiqiang Xia [a,b], Jinjian Ding [a,b], Minjie Li [a,b,**], Liang-Hong Guo [a,b,*]

[a] College of Quality and Safety Engineering, China Jiliang University, Hangzhou, Zhejiang, 310016, PR China
[b] Institute of Environmental and Health Sciences, China Jiliang University, Hangzhou, Zhejiang, 310016, PR China
[c] College of Life Sciences, China Jiliang University, Hangzhou, Zhejiang, 310016, PR China

ARTICLE INFO

Keywords:
Photoelectrochemical assay
γH2AX
Genotoxicity
Bi_2WO_6
Oxygen vacancies

ABSTRACT

Toxicity screening and risk assessment of an overwhelmingly large and ever-increasing number of chemicals are vitally essential for ecological safety and human health. Genotoxicity is particularly important because of its association with mutagenicity, carcinogenicity and cancer. Phosphorylated histone H2AX (γH2AX) is an early sensitive genotoxic biomarker. It is therefore highly desirable to develop analytical methods for the detection of trace γH2AX to enable screening and assessment of genotoxicity. Here, we developed a novel cathodic photoelectrochemical (PEC) immunoassay with dual signal amplification for the rapid and ultrasensitive detection of γH2AX in cell lysates. A sandwich immuno-reaction targeting γH2AX was first carried out on a 96-well plate, using a secondary antibody/gold nanoparticle/glucose oxidase conjugate as the labeled detection antibody. The conjugate increased the production of H_2O_2 and thus provided the first mechanism of signal amplification. The immuno-reaction product containing H_2O_2 was then detected on a photocathode prepared from $Bi_{2+x}WO_6$ rich in oxygen vacancies, with H_2O_2 acting as electron acceptor. The oxygen vacancies acted as both adsorption and activation sites of H_2O_2 and thus enhanced the photocurrent, which provided another mechanism of signal amplification. As a result, an ultrasensitive immunoassay for γH2AX determination was established with a limit of detection of 6.87 pg/mL (S/N = 3) and a wide linear range from 0.01 to 500 ng/mL. The practicability of this assay was verified by detecting γH2AX in cell lysates exposed to known genotoxic chemicals. Our work offers a promising tool for the screening of genotoxic chemicals and opening a new avenue toward environmental risk assessment.

1. Introduction

With the rapid development of social economy, an overwhelmingly large and ever-increasing number of chemicals (i.e. over 83000 chemicals in production in 2010) flow into our daily life and some became widespread environmental contaminants, posing ecological and health risks (Lan et al., 2016). Genotoxic chemicals can directly or indirectly damage cellular DNA, and cause gene mutation or mutagenesis *in Vivo*, ultimately leading to tumors or cancers (Lan et al., 2016). This renders the genotoxicity assessment a particularly important part of the chemicals' safety assessment. Traditional genotoxicity evaluation methods rely on animal experiments, but the complicated operation, long cycle and high cost seriously restrict their application in chemical safety assessment (Qu et al., 2020). With the proposal of "3 R" principle and alternative strategy of toxicity tests in the 21st century, *in Vitro* tests such as Ames test, TK test and micronucleus test have been well developed and applied (Kopp et al., 2019), but they all to some extent suffer from low specificity and sensitivity. Furthermore, even though the experiment cycle is shortened to a few days, these methods still cannot meet the need for rapid screening of large quantities of chemicals. There is a pressing need for less costly, more rapid, and reliable genotoxicity screening and testing methods.

In recent years, aiming to reduce the reliance on animal models and cell assays, biomarker-based molecular genotoxicity assays are becoming the mainstream of genotoxicity assessment. Specifically, when DNA damage occurs (i.e. DNA adducts, strand breaks, point

* Corresponding author. College of Quality and Safety Engineering, China Jiliang University, Hangzhou, Zhejiang, 310016, PR China.
** Corresponding author. College of Quality and Safety Engineering, China Jiliang University, Hangzhou, Zhejiang, 310016, PR China.
E-mail addresses: mjli@cjlu.edu.cn (M. Li), lhguo@cjlu.edu.cn (L.-H. Guo).

https://doi.org/10.1016/j.bios.2022.115052
Received 26 October 2022; Received in revised form 21 December 2022; Accepted 28 December 2022
Available online 29 December 2022

mutations, and structural and numerical chromosomal changes) (Lan et al., 2016), especially double-strand breaks (DSBs, the most severe DNA damage), the C-terminal S-139 position of histone H2AX is rapidly phosphorylated to form phosphorylated histone H2AX (γ-H2AX) (Kopp et al., 2019). The protein aggregates at DSBs sites and forms foci, and the foci number of γ-H2AX is proportional to the number of DSBs, thus making γ-H2AX a biomarker specifically characterizing DNA damage and a specific effect indicator of genotoxicity (Bernacki et al., 2016). Hitherto, various techniques have been developed for γ-H2AX detection, including gel electrophoresis (GE), HPLC-MS and immuno-technology such as western blotting (WB), immunofluorescence microscopy (IFM), and flow analysis (FA) (Rahmanian et al., 2021). Regrettably, these methods still suffer from some drawbacks. For example, the preparation of extracted proteins for WB and cell fixation as to FA or complex sample pre-processing for HPLC-MS or immunocytochemical analysis are tedious and burdensome, which greatly limit their practical application in rapid analysis of large-scale sample. As an alternative, enzyme-linked immunosorbent assay (ELISA) (Matsuzaki et al., 2010) has been developed as an easy and rapid quantification assay. However, it suffers from limited dynamic range and low sensitivity, unfavorable to its use in protein samples with a wide concentration range. Compared with ELISA, biosensors not only possess the advantages of rapid detection and easy operation but also can realize high-performance analysis by designing intelligent signal amplification strategies. Recently, our group constructed an electrochemiluminescence (ECL) immunosensor for γH2AX detection by combining the immunoassay method with a 96-electrode well plate and a high-throughput ECL detector independently developed in our laboratory (Liu et al., 2021a). Although a wide linear range of 0.2–100 ng/mL was realized, the detection limit of 200 pg/mL still cannot meet the need for low-abundance detection, especially for the low level γH2AX in the early stages of DNA damage (Bonner et al., 2008). Therefore, rapid and ultrasensitive biosensing assays are urgently needed for accurate and reliable γH2AX detection.

Similar to ECL, photoelectrochemical (PEC) bioanalysis is also developed from electrochemistry but owns a lower background signal and a higher analytical sensitivity owing to its complete separation of excitation source (light) and detection signal (electric). Especially, the cathodic PEC sensor, a photocathode detection method based on p-type semiconductors, possesses stronger anti-interference ability, since photogenerated reduction reaction, not oxidation, occurs at the photocathode/electrolyte interface (Xu et al., 2019). Therefore, the cathodic PEC sensor is more suitable for detecting low-abundance protein γH2AX in actual biological samples. However, the cathodic PEC sensor develops slowly because of the severe electron-hole pair recombination in p-type semiconductors, and the resulting weak photocurrent response and low sensitivity. Fortunately, the sensitivity of cathodic PEC sensors can be significantly improved by developing cathod materials with excellent PEC performance and designing innovative signal-amplified systems. For instance, Tang's group (Zhang et al., 2018) fabricated a Cu-doped $Zn_{0.3}Cd_{0.7}S$ as the photocathode, and the immunosensor constructed based on it for prostate-specific antigen (PSA) analysis exhibited excellent PEC performance with a detection limit of 16.3 pg/mL. Furthermore, our group (Zhang et al., 2020) designed a novel self-powered signal amplified system based on dual-photoelectrode strategy, which realized the ultrasensitive detection for human epididymal protein 4 (HE4). Therefore, preparing excellent photoactive materials coupling intelligent signal amplification strategy is vital to improve the cathodic PEC sensor performance.

For cathodic materials development, common strategies focus on improving the charge separation efficiency of materials such as element doping and hetero/homo-junction construction (Xu et al., 2019). In fact, the efficient reduction of electron acceptors (i.e. O_2 or H_2O_2) is equally important, because it determines the interfacial reaction dynamics, which in turn significantly affects the detection sensitivity. However, rather limited efforts have been exerted in this regard. Oxygen vacancies (OVs), as a point defect, can narrow the band gap, and facilitate the separation of the photo-generated charges (Wang et al., 2019). As such, they are widely introduced in metal-oxide semiconductors to enhance their PEC performance. For example, Cui et al., (2022), prepared TiO_2 nanotube with abundant OVs, compared to pristine TiO_2, the composite photocatalyst exhibited a remarkably enhanced photocurrent and lower detection limit (0.33 nmol/L) for tetracycline hydrochloride. Besides,

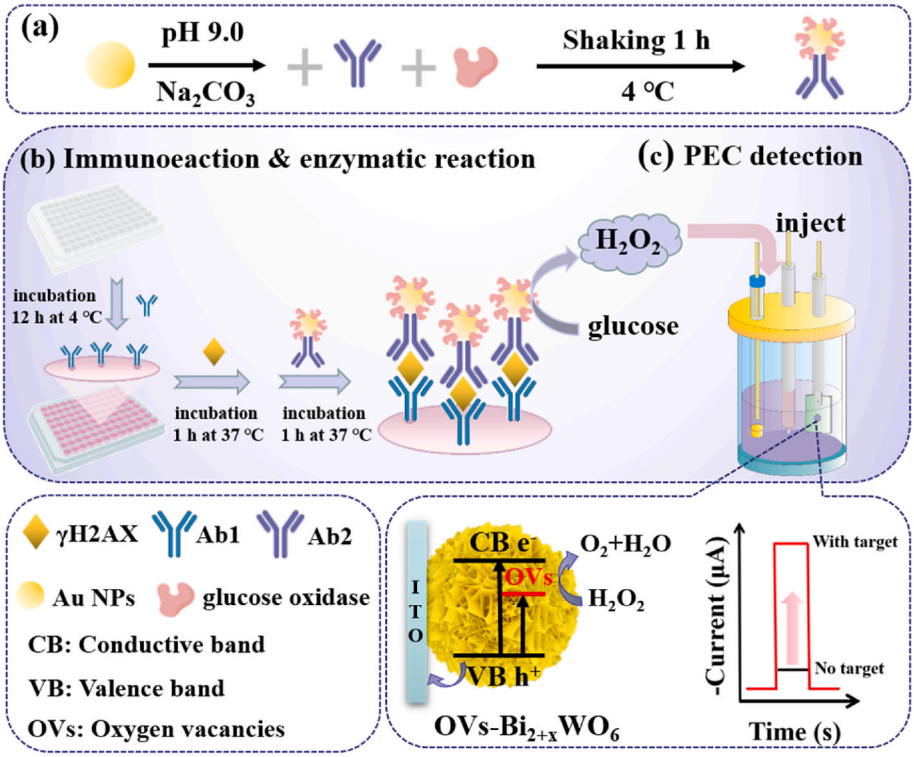

Scheme 1. Schematic illustration of the split-type PEC immunoassay for γH2AX detection.

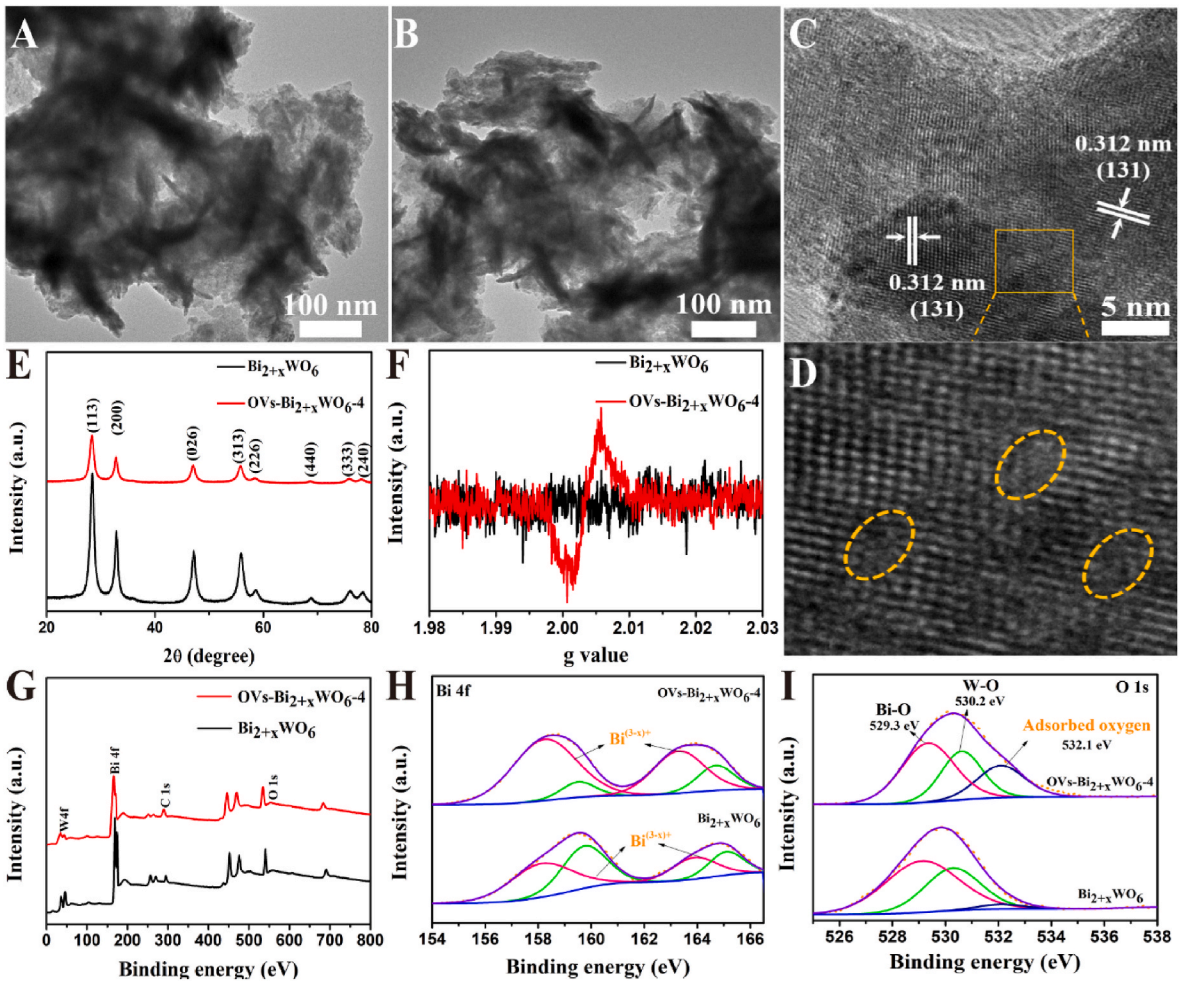

Fig. 1. TEM images of $Bi_{2+x}WO_6$ (A) and OVs-$Bi_{2+x}WO_6$-4 (B). (C) HRTEM image and partially enlarged image (D) of OVs-$Bi_{2+x}WO_6$-4. (E–I) XRD, ESR, XPS survey spectra, high-resolution Bi 4f and O 1s XPS spectra of two samples.

the abundant localized electrons on the surface of the photocatalyst endowed by the OVs can activate and even dissociate small molecules like O_2 and H_2O_2, accelerating the interfacial reaction dynamics, and thus further raising the sensitivity of cathodic PEC sensor. Interestingly, it was reported that compared to O_2, H_2O_2 was more easily induced dissociation by the localized electrons on OVs, because the single O–O bond in H_2O_2 is much weaker than the O═O double bond in O_2 (Li et al., 2017). Also, it has been proven that H_2O_2 has a greater impact on cathodic photocurrent than O_2 (Wang et al., 2019). Therefore, it is an intelligent strategy to improve the sensitivity of the cathodic PEC sensor by introducing OVs in cathodic materials to activate electron acceptor H_2O_2.

Besides the effect of photoelectrode materials, the signal amplification strategy is also related to sensitivity. For PEC immunoassays, commonly used signal amplification strategies rely on the steric hindrance effect realized by immobilization-based PEC sensing mode due to its simple principle. However, in a conventional immobilization-based PEC immunoassay, the sample incubation must be carried out on the modified electrode which determines its time-consuming and low protein loading. Moreover, target-recognition probes fastened to the electrode surfaces, such as proteins and enzymes may be impaired by light irradiation, thereby resulting in poor stability and low sensitivity (Wang et al., 2020). To overcome the above drawbacks, immobilization-free sensors developed (Lv et al., 2021; Xu et al., 2020). The immobilization-free strategy allows for a split-type detection mode. In a split-type design, the immunoreaction and the PEC detection are conducted in separate vessels, and the bridge between the two parts is usually a signal-amplification strategy in which enzymes coupled to the immunoreaction catalyze the in-situ generate generation of electron acceptors (i.e. H_2O_2). Thus, the spilt-type mode has dual merits. First, it eliminates mutual interference between biological recognition and PEC detection system, so that highly sensitive and rapid analysis are possible. Second, it contributes to the enhanced reliability endowed by the "signal-on" format, owing to its lower false positive results compared to the "signal-off" cathodic one.

Inspired by these facts, we designed a rapid and ultrasensitive cathodic PEC immunoassay for the detection of γH2AX in cells by using photoactive material with abundant OVs as photocathode and the glucose oxidase (GO*x*) mediated in-situ generated electron acceptor H_2O_2 for dual-signal amplification. In this strategy, $Bi_{2+x}WO_6$ (Bi-doped Bi_2WO_6) was chosen as photocathode and OVs regulated $Bi_{2+x}WO_6$ (donated as OVs-$Bi_{2+x}WO_6$) was prepared by glyoxal-assisted hydrothermal method, where glyoxal acted as a mild reducing agent to generate OVs. The mechanism of OVs for enhancing the PEC performance of $Bi_{2+x}WO_6$ was in-depth discussed. Then OVs-$Bi_{2+x}WO_6$ photocathode was combined with GO*x*-mediated immunoreaction performed in microplates to construct a split-type cathodic PEC immunosensor assay for the highly sensitive and rapid analysis of γH2AX.

2. Experimental section

Experimental section includes regents, instruments, preparation of materials, immunoreaction procedure and PEC detection were in supporting information (SI).

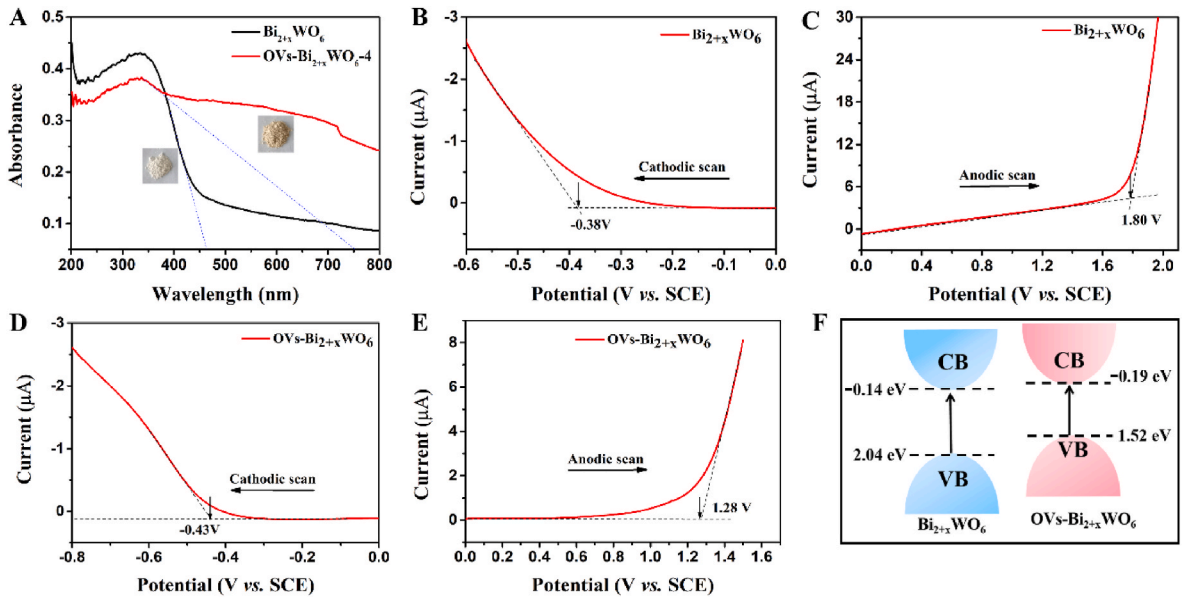

Fig. 2. (A) UV–vis DRS of two samples. Cathodic and anodic linear potential scan for determining the CB and VB of $Bi_{2+x}WO_6$ (B, C) and OVs-$Bi_{2+x}WO_6$-4 (D, E). Experiments were conducted in N_2-saturated PBS (10 mmol/L, pH 7.4). (F) Schematic of energy band positions.

3. Results and discussion

3.1. Design and construction of the split-type PEC immunoassay

As presented in Scheme 1, the split-type PEC immunoassay consisted of an immunoassay based on enzymatic reaction (Scheme 1b) and a PEC detection (Scheme 1c). Firstly, Ab2-AuNPs-GO*x* (Scheme 1a) as the detection tag was introduced in 96 microplates coated with Ab1 via specific recognition between Ab2 and γH2AX to construct a sandwich immunorecognition assay format. With the aid of GO*x*, glucose underwent fast hydrolysis to produce H_2O_2. The resultant solution was then transferred into a PEC cell, where the H_2O_2 acted as an electron acceptor that could be reduced by the photogenerated electrons on the conductive band (CB) of OVs-$Bi_{2+x}WO_6$. This process could improve charge separation efficiency, and result in enhanced photocurrent response. Particularly, there was a large number of active regions on the surface of OVs-$Bi_{2+x}WO_6$ endowed by OVs. These active regions could preferentially adsorb H_2O_2, and then be activated by the abundant localized electrons on them. Thus, the reductive reaction of H_2O_2 on the OVs-$Bi_{2+x}WO_6$ photoelectrode was promoted, and the cathodic photocurrent signal was further amplified. Finally, ultrasensitive γH2AX determination was achieved.

3.2. Characterization of the PEC immunoassay

The synthesis and characterization of immunoassay-related materials were described in SI. $Bi_{2+x}WO_6$ (i.e. Bi self-doped Bi_2WO_6) has been proven to be a novel cathodic material owing to the p-n homojunction property produced by Bi doping in our previous work, but its photocurrent could not still meet the need of sensing because of severe photogenerated charge recombination (Zhang et al., 2020). Herein, we adopted the strategy of introducing OVs to enhance its PEC performance. So far, calcination, solvothermal treatment, surfactant-assisted synthesis and plasma method have been adopted to introduce OVs into semiconductors (Zhu et al., 2020). However, it is currently challenging to regulate the contents of OVs in a controlled manner, which is crucial in photocathodic sensing applications. Specifically, the reduction of H_2O_2 will be restricted when the concentration of surface OVs is too low, whereas the photocurrent signal is reduced when there are too many surface OVs because they operate as a center of charge recombination (Ge et al., 2019). In this work, OVs-$Bi_{2+x}WO_6$ photocatalysts were prepared using a one-step hydrothermal approach assisted by glyoxal, wherein glyoxal served as the reducing agent to produce OVs. The contents of OVs were controlled by changing the glyoxal concentrations and its effect was researched by testing the photocurrent of OVs-$Bi_{2+x}WO_6$ synthesized at different concentrations of glyoxal. As seen from Fig. S2A, with increasing glyoxal concentrations, the photocurrent grew and peaked at 0.075 mol/L (sample marked as OVs--$Bi_{2+x}WO_6$-4). When the concentration continued to increase, the photocurrent gradually decreased, indicating the OVs contents were in excess. Therefore, the OVs content in OVs-$Bi_{2+x}WO_6$-4 was most suitable. Next, the stability of OVs-$Bi_{2+x}WO_6$-4 was researched, as presented in Fig. S2B, the photocurrent of OVs-$Bi_{2+x}WO_6$-4 based photoelectrode presented excellent stability during five cycles in absence of electron acceptor, which could completely satisfy the sensing need and in turn demonstrated the glyoxal-assisted hydrothermal approach was reliable and effective. Thus OVs-$Bi_{2+x}WO_6$-4 was representative for the following characterizations and experiments.

The morphologies and structures of $Bi_{2+x}WO_6$ and OVs-$Bi_{2+x}WO_6$-4 were characterized using TEM and HRTEM. As shown in Fig. 1A and B, before and after doping OVs, $Bi_{2+x}WO_6$ revealed a similar stacked nanosheet morphology. To confirm the successful introduction of OVs, HRTEM was performed. As seen in Fig. 1C, the lattice spacing was 0.312 nm, corresponding to the (113) lattice plane of the Bi_2WO_6 phase (Liu et al., 2021b). Importantly, some certain lattice disorders in the crystal lattice of Bi_2WO_6 could be observed from a partially enlarged HRTEM (Fig. 1D), which was the direct evidence of the presence of OVs (Yang et al., 2022). Fig. 1E showed the XRD spectra of $Bi_{2+x}WO_6$ and OVs--$Bi_{2+x}WO_6$-4 samples. Apparently, all the diffraction peaks in the two samples could match well with the orthorhombic phase of Bi_2WO_6 (JCPDS 39–0256) (Liu et al., 2021b). However, compared to $Bi_{2+x}WO_6$, the peak intensity of OVs-$Bi_{2+x}WO_6$-4 was significantly reduced, indicating that there were plentiful defects in the OVs-$Bi_{2+x}WO_6$-4. To further confirm the formation of OVs, ESR was performed. As presented in Fig. 1F, the OVs-$Bi_{2+x}WO_6$-4 exhibited an obvious EPR signal at $g = 2.003$ compared with $Bi_{2+x}WO_6$, revealing that OVs existed in OVs--$Bi_{2+x}WO_6$-4 after glyoxal reduction (Wang et al., 2019). Simultaneously, the increase of peak areas of low valence $Bi^{(3-x)+}$ in Bi 4f XPS spectra and adsorbed oxygen in O 1s XPS spectra also supported the presence of OVs (Fig. 1G–I) (Geng et al., 2018; Yang et al., 2022). These also

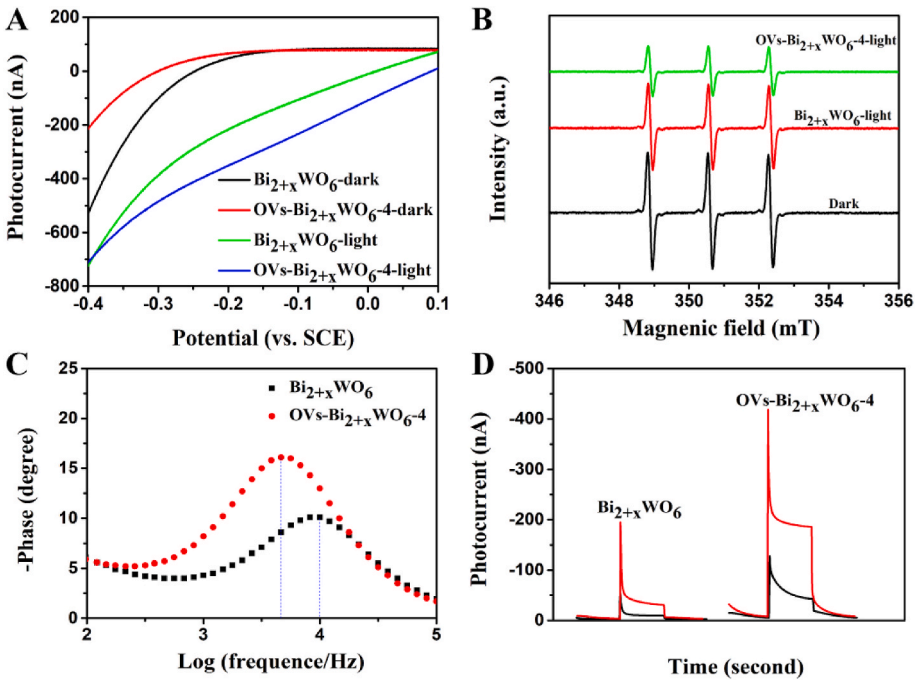

Fig. 3. (A) I–V curves, TEMPO-h^+ ESR spectra (B), and Bode phase plots (C) of two samples. (D) Photocurrent responses of two samples with (red line) or without (black line) 10 nmol/L H_2O_2.

demonstrated that glyoxal reduction was a reliable and effective method to introduce OVs.

Generally, the introduction of OVs could alter the material's light absorption properties. Thus, UV–vis DRS was conducted to explore the change in optical absorption before and after introducing OVs in $Bi_{2+x}WO_6$. As shown in Fig. 2A, the OVs-$Bi_{2+x}WO_6$-4 displayed a significant red-shift absorption edge (~750 nm) than $Bi_{2+x}WO_6$ (~460 nm), which was consistent with the color change from white to brown (the inset in Fig. 2A). Additionally, compared with $Bi_{2+x}WO_6$, the OVs-$Bi_{2+x}WO_6$-4 showed an obviously enhanced absorption intensity that derived from the abundant surface OVs (Zhu et al., 2020). The CB and VB of $Bi_{2+x}WO_6$ and OVs-$Bi_{2+x}WO_6$-4 were investigated by electrochemical method (Fig. 2B–E). The results showed that, $Bi_{2+x}WO_6$ had a CB edge at −0.38 V and a VB edge at 1.80 V *vs.* SCE, and OVs-$Bi_{2+x}WO_6$ had a CB edge at −0.43 V and a VB edge at 1.28 V *vs.* SCE. That is, the CB and VB potentials of $Bi_{2+x}WO_6$ were −0.14 and 2.04 V *vs.* NHE, and those of OVs-$Bi_{2+x}WO_6$ were −0.19 V and 1.52 V *vs.* NHE, respectively. Compared to the CB potential of $Bi_{2+x}WO_6$, the upshifted CB position of OVs-$Bi_{2+x}WO_6$-4 could more effectively reduce H_2O_2, and further improve the sensitivity. The band-gap energies (E_g) were calculated by the equation of $E_g = E_{VB} - E_{CB}$. The E_g of OVs-$Bi_{2+x}WO_6$-4 was 1.71 eV, which was narrower than that of $Bi_{2+x}WO_6$ (2.18 eV). This phenomenon could be attributed to the introduction of OVs, which caused sub-excitation from defect states to the CB (Zhu et al., 2020). In other words, surface OVs effectively narrowed the band gap of $Bi_{2+x}WO_6$ and reduced the excitation energy requirement. Fig. 2F showed the difference of energy band positions between $Bi_{2+x}WO_6$ and OVs-$Bi_{2+x}WO_6$-4. Based on the above DRS and energy band potentials analysis, it could be concluded that OVs could increase light absorption, narrow the bandgap, and enhance the photoreduction capacity of $Bi_{2+x}WO_6$.

3.3. Evaluation of PEC enhancement performance

To further investigate the effect of OVs on the separation and recombination of the photogenerated charges, electrochemical and photoelectrochemical tests were performed. As illustrated in Fig. 3A, the OVs-$Bi_{2+x}WO_6$-4 presented a significantly higher cathodic photocurrent than $Bi_{2+x}WO_6$ under irradiation. This phenomenon indicated that much more photoexcited holes were produced for OVs-$Bi_{2+x}WO_6$-4, which was directly proved by ESR spectra (Fig. 3B). TEMPO was used to capture h^+, the TEMPO signals of two samples were greatly reduced under light, indicating that holes were generated by the catalysts. Additionally, the reduction degree of OVs-$Bi_{2+x}WO_6$-4 was greater than that of the $Bi_{2+x}WO_6$, demonstrating that much more photoexcited holes were produced for OVs-$Bi_{2+x}WO_6$-4. Moreover, the significantly enhanced PEC performance of OVs-$Bi_{2+x}WO_6$-4 was further confirmed by the EIS test. As shown in Fig. S3A, under light irradiation, the arc radius of OVs-$Bi_{2+x}WO_6$-4 was smaller than that of $Bi_{2+x}WO_6$, demonstrating that the OVs in OVs-$Bi_{2+x}WO_6$-4 decreased the interfacial resistance and increased electrical conductivity. Furthermore, the Bode tests were conducted to investigate the electron lifetime of the photocatalysts. As observed from Fig. 3C, the peak frequencies of $Bi_{2+x}WO_6$ and OVs-$Bi_{2+x}WO_6$-4 were 10000 and 4677.4 Hz, respectively. Using the equation of $\tau_e = 1/(2f_{max})$ (τ_e represents the electron lifetime), the τ_e of $Bi_{2+x}WO_6$ and OVs-$Bi_{2+x}WO_6$-4 were 15.9 and 34.0 μs, respectively. Compared to $Bi_{2+x}WO_6$, the τ_e of OVs-$Bi_{2+x}WO_6$-4 doubled, indicating that OVs-$Bi_{2+x}WO_6$-4 possessed higher charge separation efficiency. This was most likely owing to the appropriate surface OVs as charge separation centers to enhance the charge separation efficiency (Hu et al., 2022). The lower PL intensity of OVs-$Bi_{2+x}WO_6$-4 also supported this point (Fig. S3B), because lower PL intensity presented a lower charge recombination degree. Therefore, we could firmly conclude that the introduction of OVs in OVs-$Bi_{2+x}WO_6$-4 indeed promoted the charge separation and enhanced the PEC performance of $Bi_{2+x}WO_6$, which laid a foundation for the improvement of detection sensitivity. To verify this point, the photocurrent responses of $Bi_{2+x}WO_6$ and OVs-$Bi_{2+x}WO_6$-4 in electrolytes with or without H_2O_2 were tested. As exhibited in Fig. 3D, the change of photocurrent value of OVs-$Bi_{2+x}WO_6$-4 was 123.9 nA in the presence and absence of H_2O_2, which was 4.9 times that of $Bi_{2+x}WO_6$, indicating that OVs-$Bi_{2+x}WO_6$-4 was more sensitive to H_2O_2 than $Bi_{2+x}WO_6$. Combine the band results above (Fig. 2D), we could conclude that, the efficient reduction of the electron receptor H_2O_2 was indeed facilitated by surface OVs, thus further amplifying the cathodic photocurrent signal, greatly improving the detection sensitivity, and

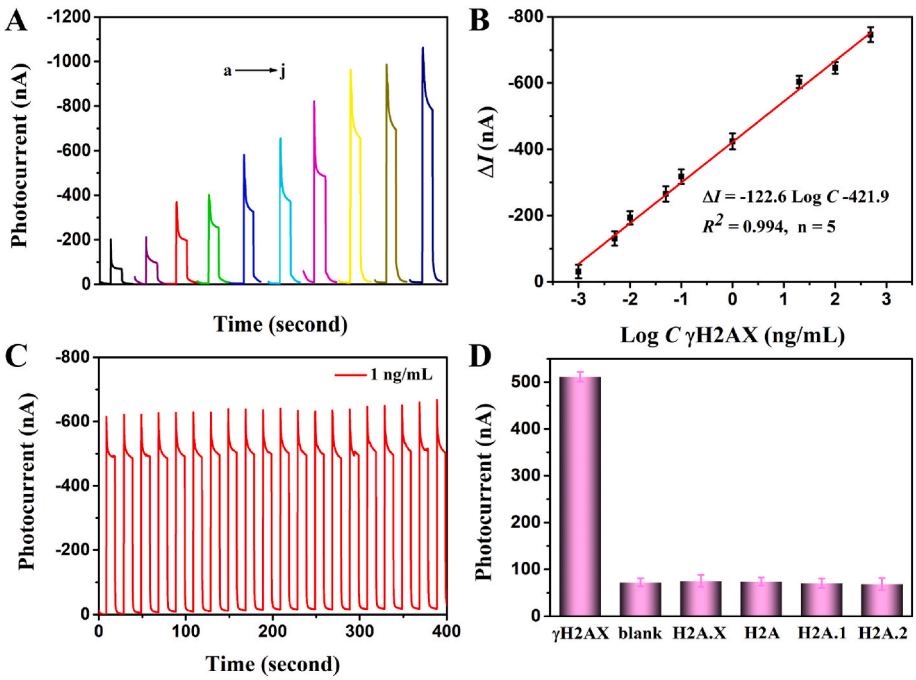

Fig. 4. (A) The photocurrent responses of the PEC immunosensor under different concentrations of γH2AX, from a to j: 0, 0.001, 0.005, 0.01, 0.05, 0.1, 1, 20, 100, 500 ng/mL. (B) The corresponding calibration curve. (C) The stability test of the PEC immunosensor of 1.0 ng/mL γH2AX. (D) Influence of coexistent substances on the PEC immunosensor in 1.0 ng/mL γH2AX and 10 ng/mL H2A.X, H2A, H2A.1, H2A.2.

ultimately achieving ultrasensitive γH2AX determination.

3.4. Analytical performance of the PEC immunoassay

Under the optimal conditions (Fig. S4), the as-constructed PEC immunoassay platform was used for the quantitative analysis of γH2AX. As displayed in Fig. 4A, the photocurrent increased with increasing γH2AX concentration. And further investigation (Fig. 4B) revealed a perfect linear relationship between the change of the photocurrent intensity (ΔI) and the logarithm of γH2AX concentration in the range of 0.001–500 ng/mL. The regression equation was ΔI (nA) = −122.6 Log$C_{\gamma H2AX}$ (ng/mL) - 421.9 (R^2 = 0.994). The detection limit was calculated as 6.87 pg/mL (S/N = 3). These are superior compared to previously reported methods for measuring γH2AX (Table S1), mainly owing to the following unique superiorities of our PEC immunoassay. First, this sensing platform exempted the need for cumbersome electrode modification steps with the aid of the split mode, thus largely saving detection time and improving detection stability. Second, owing to the dual signal amplification strategies of in-situ generation electron acceptor H_2O_2 and OVs activation, the proposed PEC immunosensor could detect as low as 6.87 pg/mL γH2AX with a wider range of 0.001–500 ng/mL, thus allowing the ultrasensitive analysis of a large difference in the γH2AX level. These above together contribute to the superior analytical performance for γH2AX quantification.

Stability is a crucial criterion for PEC immunosensors and it was explored here. As seen from Fig. 4C, under repeated external switching irradiation for more than 400 s, the intensity and shape of the photocurrent response to γH2AX (1 ng/mL) were relatively stable, indicating good stability of the PEC biosensor. After two weeks of storage at 4 °C, the photocurrent intensity of this sensor only decreased by 3.3%, indicating that the stability was satisfied. To analyze the producibility of the PEC immunoassay, five independent sensors were incubated with 1.0 ng/mL γH2AX, and the RSD was 2.98%, which was acceptable for immunosensors.

To explore the specificity of the PEC immunosensor, several proteins of the same family as γH2AX including unphosphorylated histone H2AX, H2A, H2A1, and H2A2 were tested. As presented in Fig. 4D, only γH2AX could specifically activate the PEC signal, demonstrating that the PEC immunosensor had excellent selectivity for target γH2AX recognition. Thus, the PEC immunoassay had satisfactory properties that favored long-term storage and transport in practical applications.

3.5. Detection of γH2AX spiked in cell lysates

The practical suitability of the PEC sensing system for γH2AX was evaluated by the standard addition method in a blank matrix obtained by the lysis of normally-cultured HepG2 cells (the culture and treatment procedures were in SI). As shown in Table S2, no γH2AX protein was detected in the blank cell lysate. When spiked with 80, 160, 320, and 640 pg/mL γH2AX, the recoveries ranged from 89.12 to 103.2%, with the RSD of 2.9–4.3%, indicating that the as-prepared PEC immunosensor was reliable and could be used for the determination of actual cell lysates samples. Besides, the samples were also detected by a commercial human γH2AX ELISA kit. The recoveries were 81.38–102.8% with an RSD of 2.5–4.7%. This further demonstrated that our constructed PEC immunosensor assay was reliable and could be used for actual sample detection. What's more, by comparing the recoveries (81.38–82.21%) of ELISA at low concentrations of γH2AX, the constructed PEC immunosensor exhibited higher recoveries of 89.12–103.2%. This result indicated our method has higher sensitivity and accuracy for the determination of low concentration γH2AX, which is more conducive to the reliable screening of genotoxic chemicals.

3.6. Detection of γH2AX in cell lysates after exposure to genotoxic compounds

To verify the practicability of the PEC immunosensor in screening genotoxic compounds, several known genotoxic chemicals were tested. It is well-known that camptothecin (CPT) and etoposide (ETP) can cause DNA DSBs at a certain concentration, while sodium chloride (NaCl) cannot (Qu et al., 2020). Thus, CPT and ETP were used as positive controls, while NaCl was used as a negative control. Initially, HepG2 cells were exposed to 10 nmol/L CPT, 1 μmol/L ETP, and 1 mmol/L NaCl for 24 h respectively, according to the cell viability assay results (Fig. S5,

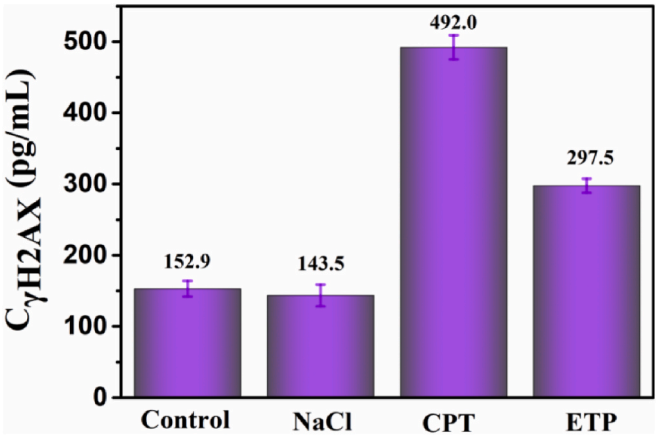

Fig. 5. Measured concentrations of γH2AX in lysate samples of HepG2 cells after 24 h exposure to 10 nmol/L CPT, 1 μmol/L ETP, or 1 mmol/L NaCl, and detected by the PEC immunoassay.

the experimental procedure was shown in SI). After exposure, Cell lysates (the total protein concentrations among treatments were close and the results were shown in Table S3) were detected by the PEC immunosensor. As presented in Fig. 5, there was a basal existence of 152.9 pg/mL γH2AX in the 0.1% DMSO control group. After treatment with CPT and ETP, the concentrations of γH2AX in HepG2 cells significantly increased 3.21- and 1.94-fold of the control, respectively, whereas exposure to NaCl showed no difference. According to the genotoxicity evaluation standard (Smart et al., 2011), that is, the level of γH2AX in the treatment group was 1.5 times higher than that in the negative control group, CPT and ETP were genotoxic substances while NaCl was not, which were in agreement with the previous study (Qu et al., 2020). These results directly and effectively proved the feasibility of the PEC immunosensor in screening genotoxic chemicals.

4. Conclusions

In this work, a rapid and ultrasensitive cathodic PEC bioanalysis platform for monitoring the γH2AX in cell lysates was designed based on a dual-signal amplification strategy and split-type detection mode. Among, high sensitivity was endowed by the dual signal amplification strategy of introduced OVs in $Bi_{2+x}WO_6$ and the in-situ generation electron acceptor H_2O_2. Specifically, experimental results demonstrated that as-prepared OVs-$Bi_{2+x}WO_6$ photocatalyst could exhibit excellent PEC performance, ultrasensitive to H_2O_2 and good photo-stability owing to the introduction of OVs. Besides, the split-type sensing mode greatly eliminated the damage of biomolecules caused by the physical light source, maintained the bioactivity of the proteins and adequately promoted the PEC efficiency of the OVs-$Bi_{2+x}WO_6$ photocatalyst. Consequently, compared with the existing detection methods for γH2AX proteins, the as-constructed cathodic PEC immunoassay platform exhibited a wider linear response range of 0.001–500 ng/mL and a much lower detection limit of 6.87 pg/mL. Furthermore, our bioanalysis platform was successfully applied to screen genotoxic chemicals, showing desirable feasibility and accuracy. As a whole, with simple processes and ultrasensitive detection properties, this work provides a promising platform for screening the genotoxicity of multitudinous chemicals. Furthermore, the as-prepared split-type PEC immunosensor was expected to realize high-throughput detection with the help of microplates in the future.

CRediT authorship contribution statement

Bihong Zhang: Conceptualization, Methodology, Formal analysis, Investigation, Writing – original draft. **Fangfang Li:** Formal analysis, Investigation. **Linyu Shen:** Formal analysis, Investigation. **Lu Chen:** Formal analysis, Investigation. **Zhiqiang Xia:** Validation, Supervision. **Jinjian Ding:** Data curation, Software, Funding acquisition. **Minjie Li:** Writing – review & editing. **Liang-Hong Guo:** Conceptualization, Writing – review & editing, Supervision, Project administration, Funding acquisition.

Declaration of competing interest

The authors declare that they have no known competing financial interests or personal relationships that could have appeared to influence the work reported in this paper.

Data availability

The authors are unable or have chosen not to specify which data has been used.

Acknowledgment

This study was supported by the National Science Foundation of China (22036005), and Zhejiang Key Research and Development Program (2021C03057).

Appendix A. Supplementary data

Supplementary data to this article can be found online at https://doi.org/10.1016/j.bios.2022.115052.

References

Bernacki, D.T., Bryce, S.M., Bemis, J.C., Kirkland, D., Dertinger, S.D., 2016. Environ. Mol. Mutagen. 57 (7), 546–558.
Bonner, W.M., Redon, C.E., Dickey, J.S., Nakamura, A.J., Sedelnikova, O.A., Solier, S., Pommier, Y., 2008. Nat. Rev. Cancer 8 (12), 957–967.
Cui, H., Yao, C.F., Cang, Y.G., Liu, W.T., Zhang, Z.H., Miao, Y.Q., Xin, Y.M., 2022. Sensor. Actuator. B Chem. 359, 131564.
Ge, L., Liu, Q., Jiang, D., Ding, L., Wen, Z., Guo, Y., Ding, C., Wang, K., 2019. Biosens. Bioelectron. 135, 145–152.
Geng, Z., Kong, X., Chen, W., Su, H., Liu, Y., Cai, F., Wang, G., Zeng, J., 2018. Angew. Chem. Int. Ed. 57 (21), 6054–6059.
Hu, X., Wang, J., Wang, J., Deng, Y., Zhang, H., Xu, T., Wang, W., 2022. Appl. Catal. B Environ. 318, 121879.
Kopp, B., Khoury, L., Audebert, M., 2019. Arch. Toxicol. 93 (8), 2103–2114.
Lan, J., Gou, N., Rahman, S.M., Gao, C., He, M., Gu, A.Z., 2016. Environ. Sci. Technol. 50 (6), 3202–3214.
Li, H., Shang, J., Yang, Z., Shen, W., Ai, Z., Zhang, L., 2017. Environ. Sci. Technol. 51 (10), 5685–5694.
Liu, C., Qie, Y., Zhao, L., Li, M., Guo, L.-H., 2021a. ACS Sens. 6 (10), 3724–3732.
Liu, T., Gu, M., Zhao, L., Wu, X., Li, Z., Wang, G.-L., 2021b. Chem. Commun. 57 (71), 8989–8992.
Lv, Z., Zhu, L., Yin, Z., Li, M., Tang, D., 2021. Anal. Chim. Acta 1171, 338680.
Matsuzaki, K., Harada, A., Takeiri, A., Tanaka, K., Mishima, M., 2010. Mutat. Res-Gen. Tox. En. 700 (1), 71–79.
Qu, M., Xu, H., Chen, J., Zhang, Y., Xu, B., Guo, L., Xie, J., 2020. Chem. Res. Toxicol. 33 (8), 2108–2119.
Rahmanian, N., Shokrzadeh, M., Eskandani, M., 2021. DNA Repair 108, 103243.
Smart, D.J., Ahmedi, K.P., Harvey, J.S., Lynch, A.M., 2011. Mutat. Res-Fund. Mol. M. 715 (1–2), 25–31.
Wang, H., Zhang, B., Tang, Y., Wang, C., Zhao, F., Zeng, B., 2020. TrAC, Trends Anal. Chem. 131, 116020.
Wang, H., Zhang, B., Xi, J., Zhao, F., Zeng, B., 2019. Biosens. Bioelectron. 141, 111443.
Xu, R., Liu, L., Liu, X., Li, Y., Feng, R., Wang, H., Fan, D., Wu, D., Wei, Q., 2020. ACS Appl. Mater. Interfaces 12 (6), 7366–7371.
Xu, Y.-T., Yu, S.-Y., Zhu, Y.-C., Fan, G.-C., Han, D.-M., Qu, P., Zhao, W.-W., 2019. TrAC, Trends Anal. Chem. 114, 81–88.
Yang, M., Xu, T., Jin, X., Shen, Q., Sun, C., 2022. Appl. Surf. Sci. 581, 152439.
Zhang, B.H., Wang, H., Xi, J.J., Zhao, F.Q., Zeng, B.Z., 2020. ACS Sens. 5 (9), 2876–2884.
Zhang, K.Y., Lv, S.Z., Lu, M.H., Tang, D.P., 2018. Biosens. Bioelectron. 117, 590–596.
Zhu, K., Shi, F., Zhu, X., Yang, W., 2020. Nano Energy 73, 104761.